Modeling of the secondary refining process of steel

D. You, S.K. Michelic and C. Bernhard, Montanuniversität Leoben, Austria

Christian Bernhard, Montanuniversität Leoben, Josef-Franz-Straße 18, +43 (0)3842-402-2220, +43 3842 402 2202, Christian.Bernhard@unileoben.ac.at

Summary
Under the background of Industry 4.0 and Integrated Intelligent Manufacturing, the process models of the secondary refining of steel are necessary to realize smart manufacturing. In the present study, the models of Ladle Furnace (LF) and Ruhrstahl Heraeus (RH) refining are developed based on the concept of linking practical metallurgical models to thermodynamic databases. In the modeling, thermodynamic library–ChemApp and ChemSage data-file are applied to perform equilibrium calculations. The effective equilibrium reaction zone (EERZ) method is used to account for the interfacial reactions. For the LF model, the tanks–in–series model is used to simply consider the mixing phenomenon. The steel/slag reaction, lining dissolution, alloy addition and air absorption are also accounted for. For the RH modeling, three reaction sites in the RH vessel are defined: bath surface, inside bath and argon (Ar) bubble surface according to the decarburization and degassing mechanism. The treatment on the reactions in the ladle during the RH refining process is similar to that in the LF modeling. The proposed models are separately validated by the already published plant data and laboratory experiments. The models can also be linked to each other to simulate the refining process. In the future, the simulations using the developed models are expected to offer references towards the online operations of the thorough process quality control of steel refining.

Key Words
Steel; refining; modeling; LF; RH; thermodynamic; kinetic

Introduction
With the demanding requirements on steel products and the development of new steel grades, the importance of the secondary refining process is becoming more and more vital. Under the background of Industry 4.0 and Integrated Intelligent Manufacturing, computational modeling is increasingly more important and popular due to its high efficiency and substantial benefits. The process models of secondary refining are valuable and necessary to control steel compositions and adjust metallurgical parameters online, which is also recognized as a digital twin. Ladle furnace (LF) and Ruhrstahl Heraeus (RH) treatments are the most widely applied approaches in the secondary refining of steel. A number of models of LF and RH processes have been proposed, and partial operations and reactions have been addressed [1-7]. The present project aims to develop comprehensive and thorough process models to simulate secondary refining process, which accounts for the various operations and metallurgical routes besides the metallurgical phenomenon in the individual metallurgical station. In the earlier research work, the continuous casting process has been modeled and applied, focusing on microsegregation, inclusion formation and hot crack formation [8-11].

In the present study, LF and RH models were developed based on the former study. Thermodynamic library–ChemApp [12] was applied to link the metallurgical models to thermodynamic databases and perform equilibrium calculations. The effective equilibrium reaction zone (EERZ) method was used to account for the interfacial reactions. Before describing the modeling process, the model concept and methods were introduced. The simulated results were compared with the industrial measurements. After summarizing the present models, the future work was outlined.

Modeling

Modeling concept
The models follow the same concept: link the easily-handled and applicable metallurgical models to thermodynamic databases. As depicted in Figure 1, various metallurgical models, such as LF, RH, microsegregation and inclusion formation, which account for both reaction thermodynamics and kinetics, are programmed using FORTRAN language. For the calculations, several initial conditions and process parameters are necessary. The thermodynamic library–ChemApp is applied to bridge the metallurgical models to thermodynamic database offered by FactSage. Thermodynamic databases can be commercial or self–optimized. In the calculation, metallurgical models provide the local compositions and conditions to ChemApp to perform equilibrium calculations, after which the desired thermodynamic data can be achieved by the subroutines of ChemApp. The thermodynamic results are also returned to the models as feedback for subsequent calculations.

Meanwhile, the effective equilibrium reaction zone (EERZ) method (Figure 2) is applied to treat multi-phase equilibrium calculations [4]. In the method, the volume of each phase in the effective reaction zone (V2 and V3) is defined by their mass transfer, as given in Equation (1). After approaching equilibrium, the phases in the reaction zone are transported back to the bulk phases (V1 and V4), respectively. This process is repeated for each interfacial reaction.

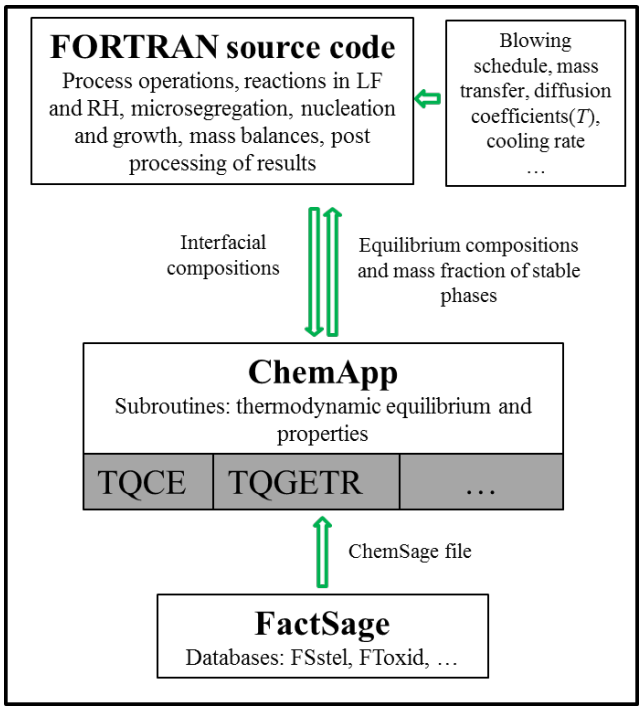

Figure 1. Modeling concept of the metallurgical processes

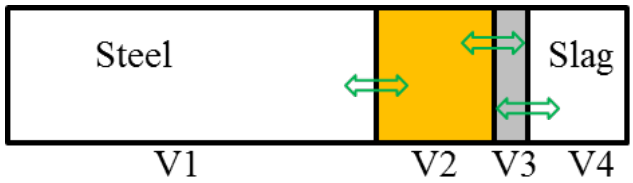

Figure 2. Schematic of the effective equilibrium reaction zone (EERZ) method for the steel/slag reaction [4]

$$\Delta V = kA\Delta t \qquad (1)$$

Where ΔV is the volume of the phase for the interfacial reaction, A is the cross section area of the interface, k is the mass transfer coefficient of the phase and Δt is the time step.

Model description

Figure 3 displays the schematic of the LF and RH models. As shown in Figure 3 (a), to consider the mixing phenomenon in a simple way, the ladle is divided into a finite number of tanks (n+1), which is the so called tanks–in–series model [13]. The number of tanks is necessary to be defined empirically. All the tanks are centrosymmetric, since the purging plug is assumed to be located in the center of the ladle bottom. The n+1st tank (plume zone of gas and steel) is regarded as a cone and the volume is defined by the empirical Equations (2) and (3) [14]. When assuming the 1st to nth tanks are the same height, the volumes of the tanks are determined. In each tank, it is assumed that the composition of steel is homogeneous. At each calculation step, the steel is transported from one tank to another in an assumed direction (black arrows). The mass flow of circulation is defined by the argon flow rate and ladle dimensions as given in Equations (4) to (6) [14-15].

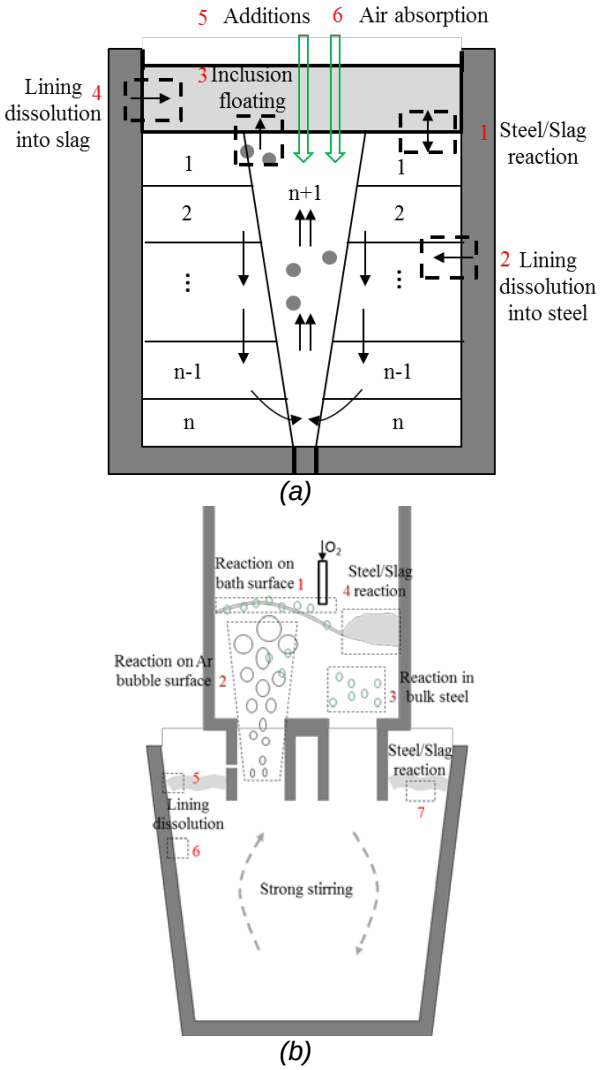

Figure 3. Schematic of the models: (a) LF and (b) RH

As displayed in Figure 3 (a), reactions 1 to 6 can be considered. The steel/slag reaction (1) happens between the tanks 1 and n+1 and the slag is treated using the EERZ method. The mass transfer coefficient of steel to the steel/slag reaction interface (k_{st}) and the rate of inclusion floating to the slag (r_{fl}) depend on the steel stirring and are calculated using the empirical Equations (7) [2] and (8) [16]. The mass transfer coefficient of slag is assumed as one of tenth

of that of steel. Lining dissolution (2 and 4) and air absorption (6) are simply accounted for by empirical rate factors. At each calculation time step, the reactions are carried out and the steel is recycled and reaches equilibrium in each tank.

$$\frac{\theta_c}{180} = 0.915 Fr_m^{0.12} (\frac{H}{D})^{-0.254} (\frac{d_n}{D})^{0.441} \quad (2)$$

$$Fr_m = \frac{16\dot{Q}^2}{\pi^2 d_n^4 g H} (\frac{\rho_G}{\rho_L - \rho_G}) \quad (3)$$

$$\dot{V}_L = 2.81 \times 10^{-3} \dot{\varepsilon}^{0.625} h^{0.942} d_n^{0.119} \quad (4)$$

$$\dot{\varepsilon} = \varepsilon * \rho_L \quad (5)$$

$$\varepsilon = (\frac{n_G RT}{m_L}) ln(\frac{P_t}{P_0}) \quad (6)$$

Where θ_c is the plume cone angle; Fr_m is the modified Froude number, as defined in Equation (2); H is the steel bath height; D is the bath diameter; d_n is the diameter of the nozzle; $\dot{Q}$ is the gas flow rate, ρ_G and ρ_L are the gas and liquid densities, respectively; π is the circumference ratio; g is the gravity acceleration. $\dot{V}_L$ is the average steel recirculation rate; $\dot{\varepsilon}$ is the rate of kinetic energy dissipation which can be calculated using Equations (5) and (6); h is the plume height; ε is the effective stirring power per unit steel; n_G is the mole of blowing Ar; R is the gas constant; T is the temperature; m_L is the mass of the liquid steel; P_t and P_0 are the gas pressure at the bottom and surface of the ladle, respectively.

$$k_{st} = (4 \pm 2) \varepsilon^{(1.4 \pm 0.09)} H \times 10^{-6} \quad (7)$$

$$r_{fl} = (5.7 \pm 1.5) \varepsilon^{(0.28 \pm 0.08)} \times 10^{-4} \quad (8)$$

In Figure 3 (b), seven reaction sites are defined for the RH model. Based on the mechanism of decarburization and degassing, three reaction sites are determined in the vacuum vessel: bath surface (1), argon (Ar) bubble surface (2) and inside bulk steel (3). It is assumed that the reaction rates on bath surface and Ar bubble surface are controlled by the mass transfer of carbon from bulk steel to the surfaces. According to the EERZ method, the effective volume of the steel for reaction sites 1 (V_{bas}) and 2 (V_{Ars}) is defined by the surface area and mass transfer coefficient of carbon (k_C, 1.5× 10^{-3} m/s [17]), as given in Equations (9) and (10). At reaction site 1, the bath surface area (A_{RH}) is significantly enlarged due to the strong stirring, gas formation and oxygen blowing and an effective factor (f in Equation (9)) is introduced to account for the effects. When there is no oxygen blowing, the effective surface area is 3.5 times that of the bath surface area ($f = 3.5$) [7]; when oxygen is blowing, the effective surface area is assumed to be 10 times that of the bath surface area ($f = 10$) [6]. For reaction site 2, the surface area of the Ar bubble is determined by the flow rate (Q_{Ar}) and the mean radius of the lifting gas, which is determined empirically. The effective reaction volume inside bulk steel (V_{bin}, reaction site 3) is determined by the height of the gas starting to form (h_r) and the cross area of the vacuum vessel as given in Equations (11) [5]. The gas formation is set as the partial pressure of the gas (P_{gas}) is larger than the total pressure of that at the half reaction depth ($\frac{\rho_L g h_r}{2} + P_v$) and the critical pressure for the formation (P_c), as described in Equation (12). A process parameter (k_a) is introduced to account for the favorable effects of the formed gas, which should be further defined according to different practices. In addition to the reaction sites 1 to 3, the steel/slag reactions (4 and 7) and lining dissolution (5 and 6) are also considered, which are similar to the calculations in the LF model. After the simulation has started, the steel is pumped into the vacuum vessel. The volume of steel in the vacuum vessel is empirically assumed based on the dimensions. The recirculation rate of steel in the vacuum vessel (Q) is calculated using Equation (13), which was summarized empirically by Kuwabara et al. [5].

$$V_{bas} = f A_{RH} k_C \Delta t \quad (9)$$

$$V_{Ars} = \frac{1}{3} \frac{Q_{Ar} \Delta t}{r_{Ar}} k_C \Delta t \quad (10)$$

$$V_{bin} = h_r A_{RH} k_a \Delta t \quad (11)$$

$$P_{gas} \geq \frac{\rho_L g h_r}{2} + P_v + P_c \quad (12)$$

$$Q = 11.4 Q_{Ar}^{\frac{1}{3}} D_u^{\frac{4}{3}} (ln(\frac{P_b}{P_v}))^{\frac{1}{3}} \quad (13)$$

Where Δt is the time step for the calculation; P_v is the pressure in the vacuum vessel; P_c is the critical formation pressure of CO, which is assumed as 0.01 atm [18]; D_u is the inner diameter of the up-snorkel, P_b is the pressure at the lifting gas blowing position.

Comparison of the calculations with industrial measurements

To evaluate the predictions from the proposed models, the calculated results were compared with the industrial measurements from literature. The calculation conditions and schedule were set as the same as those of the practice, which were described in detail elsewhere [3-4, 7, 19] . Comparisons of the simulated and measured results of the LF treatment are shown in Figure 4. It is found that the simulated results of steel (Figure 4 (a)) and slag (Figure 4 (b)) compositions agree well with the measured results. The evolutions of steel and slag correspond well with the operations. In Figure 4 (a), Al increases sharply after the first deoxidation, after which concentrations of Si, Mn, S and Al change relatively rapidly until 450 s, due to the strong blowing and steel/slag reaction.

The soft blowing from 450 s to 1140 s lowers the reaction rate. The second deoxidation (1140 s) leads to the Al and Mn concentrations soaring. Afterwards, a fast reaction rate is observed with the increasing Ar blowing. At the late stage, the changes in steel compositions are slowed down because of the decreasing Ar flow rate. For slag compositions (Figure 4 (b)), the changes also correspond closely with the operations. The good agreement of the simulated and measured results indicates that the proposed model can be applied to simulate the LF refining process.

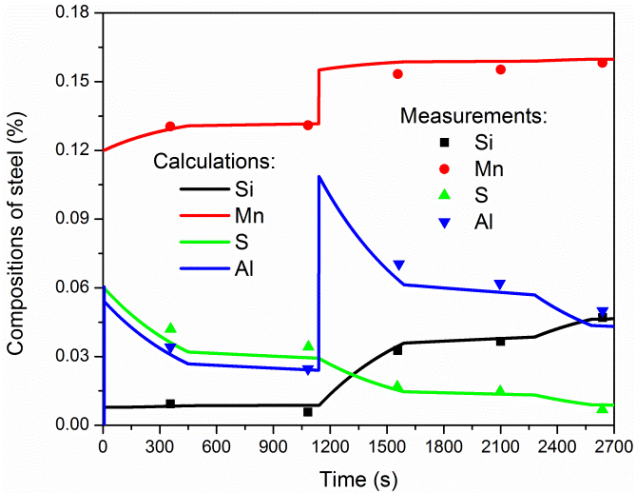

Figure 4. Comparisons of the simulated and measured results of the LF treatment: (a) steel and (b) slag compositions [3-4]

Figure 5 displays the calculated and measured C and O concentrations during the RH refining process. In the simulation, the steel pumped into the vacuum vessel was set as 21×10^3 tons [19]; the process parameter for decarburization inside the steel bath of the vacuum vessel was taken as 5 m/s. Here, RH was applied for decarburization. It can be seen that the predicted C and O concentrations fit well with the industrial measurements. Before the oxygen blowing (60 s), the decarburization rate is quite limited, while the O content increases a bit due to the steel/slag reaction. From 60 s to 240 s, with oxygen blowing, O content increases and C content decreases. After oxygen blowing, C and O contents decrease due to the lowering pressure and the formation of CO. After 440 s, the decarburization rate slows down because of the low carbon content. By comparing the simulated results of RH refining with the industrial data, the reasonability of the calculations from the proposed model is illustrated.

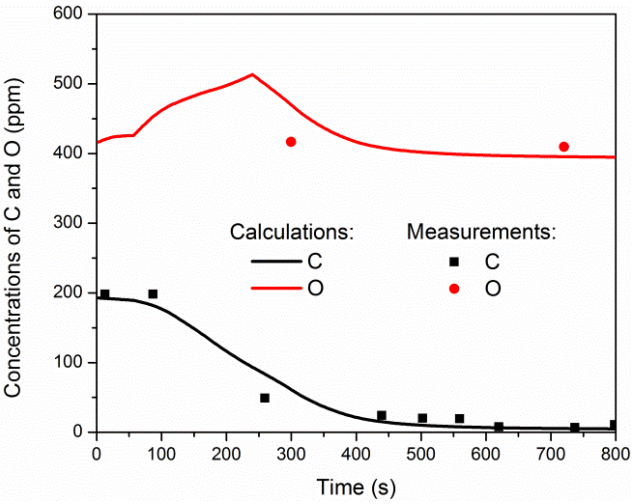

Figure 5. Calculated and measured C and O concentrations during RH process [7]

Summary and outlook

Based on the concept of linking practical models to thermodynamic databases, the models of the LF and RH processes were developed. By comparing the simulations with the industrial measurements, the validity of the models was illustrated. Note that the models can be connected and applied to simulate a thorough refining process while it was separately introduced. In future work, the models will be further improved and completed by comparing them with the big data collected from industrial partners. Meanwhile the subsequent processes such as tundish and casting will be modeled and integrated using similar techniques. The final target is to apply the modeling work as a digital twin to smart steel manufacturing.

Abbreviations

Abbreviation	Meaning
LF	Ladle furnace
RH	Ruhrstahl Heraeus
V1, V2, V3, V4	Volumes of phases
Si	Silicon
Mn	Manganese
Al	Aluminum
EERZ	Effective equilibrium reaction zone
Ar	Argon
C	Carbon
S	Sulfur
O	Oxygen
CO	Carbon monoxide

Symbol	Meaning
ΔV	The volume of the phase for interfacial reaction
A	The cross section area of interface
k	The mass transfer coefficient of the phase
H	Steel bath height
D	Steel bath diameter
d_n	Diameter of the nozzle
π	Circumference ratio
g	Gravity acceleration
$\dot{V}_L$	The average steel recirculation rate
R	Gas constant
T	Temperature
m_L	Mass of the liquid steel
r_{fl}	The rate of inclusion floating to the slag
V_{bas}	Effective reaction volume on the bath surface
V_{Ars}	Effective reaction volume on the argon bubble surface
Q_{Ar}	Flow rate of the lifting gas
V_{bin}	Effective reaction volume inside the steel bath of vacuum vessel
h_r	The height from the bath surface of gas starting to form (h_r)
P_v	The pressure in the vacuum vessel
D_u	The inner diameter of up-snorkel
Δt	Time step
θ_c	The plume cone angle
Fr_m	The modified Froude number
$\dot{Q}$	The flow rate of bottom blowing gas
ρ_G	Density of the blowing gas
ρ_L	Density of liquid steel
$\dot{\varepsilon}$	The rate of kinetic energy dissipation
ε	The effective stirring power per unit steel
n_G	The mole of bottom blowing argon
P_t	The gas pressure at the bottom of the ladle
P_0	The gas pressure on the surface of the ladle
k_{st}	Mass transfer coefficient of steel
k_C	Mass transfer coefficient of carbon in liquid steel
A_{RH}	Bath surface area of the vacuum vessel
f	An effective factor for surface area enlargement
k_a	Process parameter for the influence of formed gas
P_{gas}	The partial pressure of the gas
P_c	The critical pressure for the gas formation
P_b	The pressure of the lifting gas blowing position

Acknowledgments

We acknowledge all the supports from the department and industrial partners. Financial support by the Austrian Federal Government (in particular from Bundesministerium für Verkehr, Innovation und Technologie and Bundesministerium für Wirtschaft, Familie und Jugend) represented by Österreichische Forschungsförderungsgesellschaft mbH and the Styrian and the Tyrolean Provincial Government, represented by Steirische Wirtschaftsförderungsgesellschaft mbH and Standortagentur Tirol, within the framework of the COMET Funding Programme is gratefully acknowledged. This work is part of the ongoing K2-MPPE project P3.36 “Advanced ESP”.

References

[1] Peter, J.; Peaslee, K.D.; Robertson, D.G.; Thomas, B.G.: Experimental Study of Kinetic Processes during the Steel Treatment at two LMF’s; AISTech, 2005, No. 1, P. 959-973

[2] Graham, K.J.; Irons, G.A.: Toward Integrated Ladle Metallurgy Control; AISTech, 2009, No. 1, P. 164-173

[3] Harada, A.; Maruoka, N.; Shibata, H.; and Kitamura, S.Y.: A kinetic model to predict the compositions of metal, slag and inclusions during ladle refining: Part 1. Basic concept and application; ISIJ int., 53-12 (2013), P. 2110-2117

[4] Van Ende, M.A.; Jung, I.H.: A kinetic ladle furnace process simulation model: effective equilibrium reaction zone model using FactSage macro processing; Metall. Mater. Trans. B, 48-1 (2017), P. 28-36

[5] Kuwabara, T.; Umezawa, K.; Mori, K.; Watanabe, H.: Investigation of decarburization behavior in RH-reactor and its operation improvement; Trans. ISIJ, 28-4 (1988), P. 305-314

[6] Takahashi, M.; Matsumoto, H.; Saito, T.: Mechanism of decarburization in RH degasser; ISIJ int., 35-12 (1995), P. 1452-1458

[7] Park, Y. G.; Yi, K. W.: Investigation of decarburization behavior in RH-reactor and its operation improvement; ISIJ int., 43-9 (2003), P. 1403-1409

[8] You, D.; Bernhard, C.; Wieser, G.; Michelic, S.: Microsegregation model with local equilibrium partition coefficients during solidification of steels; Steel Res. Int., 87-7 (2016), P. 840-849

[9] You, D.; Michelic, S.K.; Bernhard, C.; Loder, D.; Wieser, G.: Modeling of inclusion formation during the solidification of steel; ISIJ int., 56-10 (2016), P. 1770-1778
[10] You, D.; Michelic, S.K.; Wieser, G.; Bernhard, C.: Modeling of manganese sulfide formation during the solidification of steel; J. Mater. Sci., 52-3 (2017), P. 1797-1812
[11] Arth, G.; Ilie, S.; Pierer, R.; Bernhard, C.: Experimental and numerical investigations on hot tearing during continuous casting of steel; BHM, 160-3 (2015), P. 103-108
[12] Petersen, S.; Hack, K.: The thermochemistry library ChemApp and its applications; Int. J. Mater. Res., 98-10 (2007), P. 935-945
[13] Levenspiel O.: Chemical Reaction Engineering, Wiley, New York 1972.
[14] Murthy, G.K.; Ghosh, A.; Mehrotra, S.T.: Mathematical modeling of mixing phenomena in a gas stirred liquid bath; Metall. Mater. Trans. B, 20-1 (1989), P. 53-59
[15] Murthy, G.K.: Mathematical modelling and simulation of recirculatory flow as well as mixing phenomena in gas stirred liquid baths; ISIJ int., 29-1 (1989), P. 49-57
[16] Graham, K.J.; Irons, G.A.: The behavior of non-metallic inclusion during ladle refining; AISTech, 2009, No. 1, P. 1003-1014
[17] Kitamura, T.; Miyamoto, K.; Tsujino, R.; Mizoguchi, S.; Kato, K.: Mathematical model for nitrogen desorption and decarburization reaction in vacuum degasser; ISIJ int., 36-4 (1996), P. 395-401
[18] You, Z.; Cheng, G.; Wang, X.; Qin, Z.; Tian, J.; Zhang, J.: Mathematical Model for Decarburization of Ultra-low Carbon Steel in Single Snorkel Refining Furnace; Metall. Mater. Trans. B, 46-1 (2015), P. 459-472
[19] Van Ende, M.A.; Kim, Y.M.; Cho, M.K.; Choi, J.; Jung, I.H.: A kinetic model for the Ruhrstahl Heraeus (RH) degassing process; Metall. Mater. Trans. B, 42-3 (2011), P. 477-489